Suppression of Coffee-ring Effect via Periodic Oscillation of Substrate for Ultra-sensitive Enrichment towards Surface-enhanced Raman Scattering

Bing Ji,[a] Lingjun Zhang,[b] Mingzhong Li,[c] Shuangpeng Wang,[a,d] Man-Kay Law,[c] Yingzhou Huang,[b] Weijia Wen,[e] and Bingpu Zhou,[a,d,*]

[a]*Joint Key Laboratory of the Ministry of Education, Institute of Applied Physics and Materials Engineering, University of Macau, Avenida da Universidade, Taipa, Macau, China*
[b]*Chongqing Key Laboratory of Soft Condensed Matter Physics and Smart Materials, College of Physics, Chongqing University, Chongqing, 400044, China*
[c]*State Key Laboratory of Analog and Mixed-Signal VLSI, University of Macau, Macau, China*
[d]*Department of Physics and Chemistry, Faculty of Science and Technology, University of Macau, Avenida da Universidade, Taipa, Macau, China*
[e]*Department of Physics, The Hong Kong University of Science and Technology, Clear Water Bay, Kowloon, Hong Kong*

Keywords: Coffee-ring effect, Suppression, Surface-enhanced Raman Scattering, Gold nanoparticle.

Corresponding Author

[*]Email: bpzhou@um.edu.mo. Fax: +853-88222426. Tel: +853-88224196.

Supporting Information

Section 1. Supporting figures

Fig. S1 shows the rough PDMS/CIP layer due to the unevenly distributed CIP. The high surface roughness may cause the pinning of NPs even in SCR system, thus a smooth layer is required to be added.

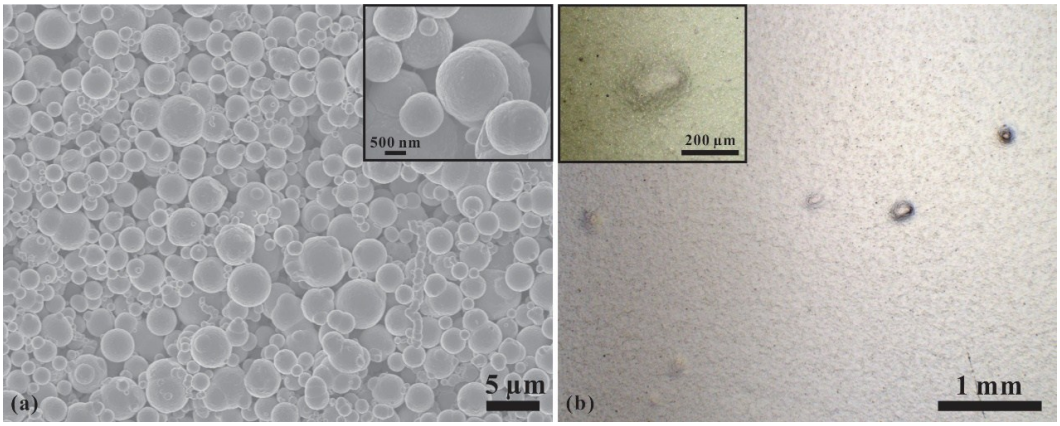

Fig. S1. SEM image of CIP (a) and optical microscope image of rough PDMS/CIP layer.

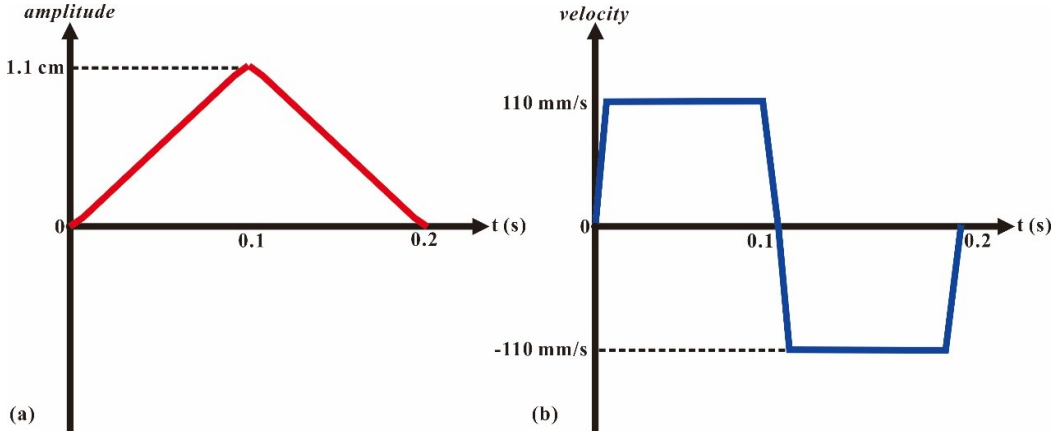

Fig. S2. Wave profiles of the amplitude (a) and velocity (b) in the reciprocating motion of the permanent magnet under driving frequency of 5.0 cycles/s.

Fig. S3 presents the change of contact angle and diameter of the sessile droplet placed statically on the magnetically functional membrane during the evaporation. Even though the substrate surface was hydrophobic, pinning of AuNPs and analyte was clearly observed during the experiment. The pinning of the droplet leads to the continuous decrease of contact angle and almost negligible change of the droplet

diameter during the evaporation process. The typical profile of the sessile droplet during such process is also shown in the interpolated plot.

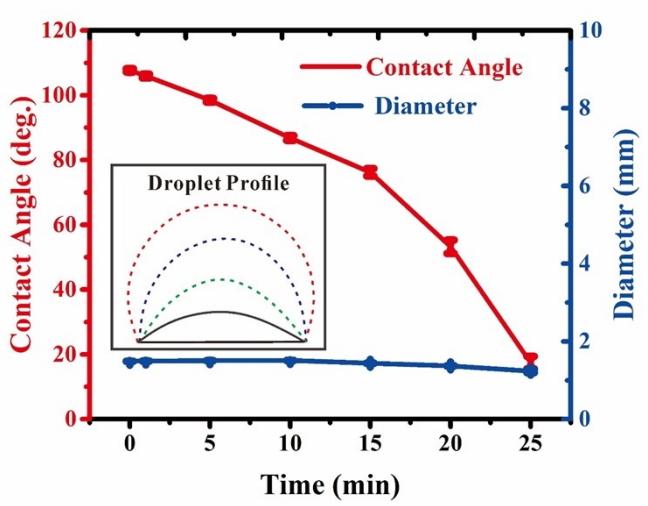

Fig. S3. Change of the contact angle and the diameter of static AuNPs/R6G suspension droplet on the magnetically functional membrane during evaporation.

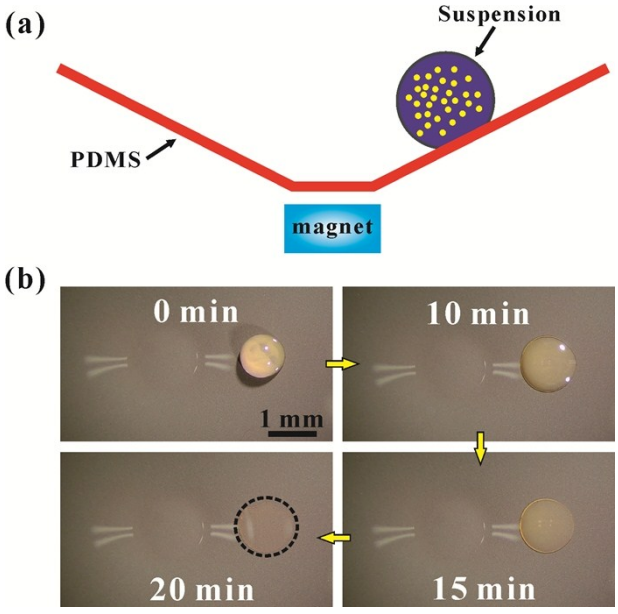

Fig. S4. (a) Experimental schematic of the suspension evaporation on the statically inclined PDMS surface. (b) Serial optical images of the AuNP assembly throughout the evaporation process.

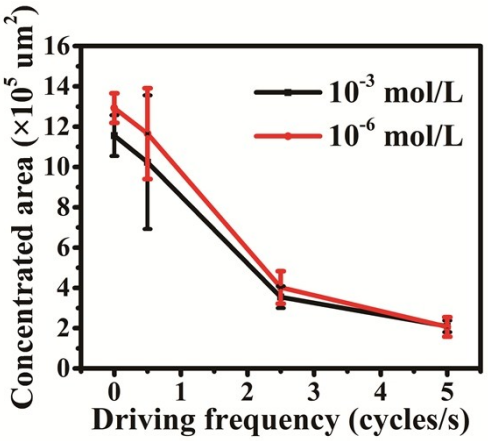

Fig. S5. Relationship between the concentrated area and driving frequency.

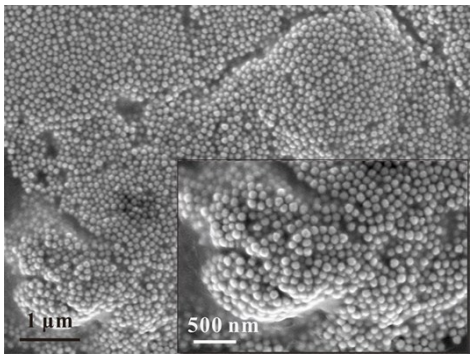

Fig. S6. SEM image of a typical aggregation of AuNPs in SCR system.

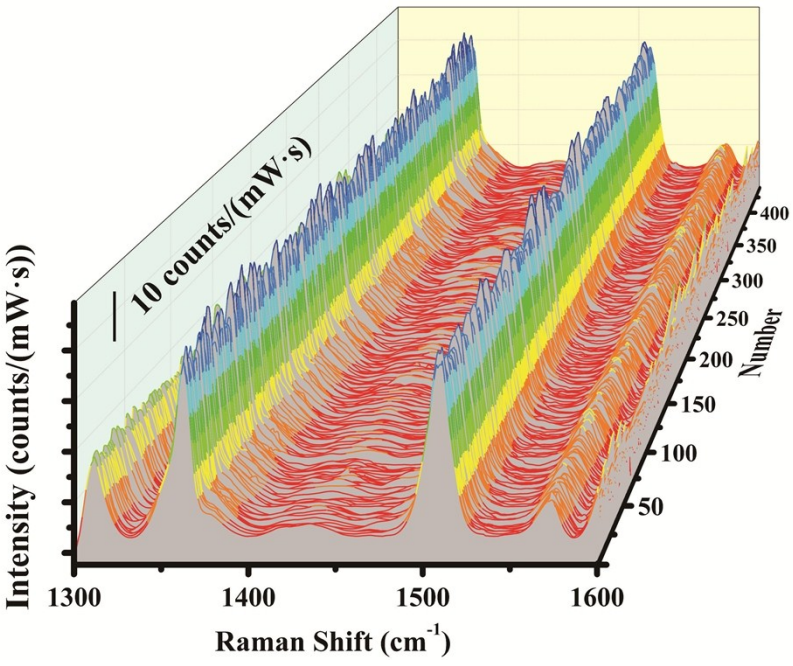

Fig. S7. Raman spectra of AuNPs/R6G (10^{-6} mol/L) in the $100\ \mu m \times 100\ \mu m$ mapping area.

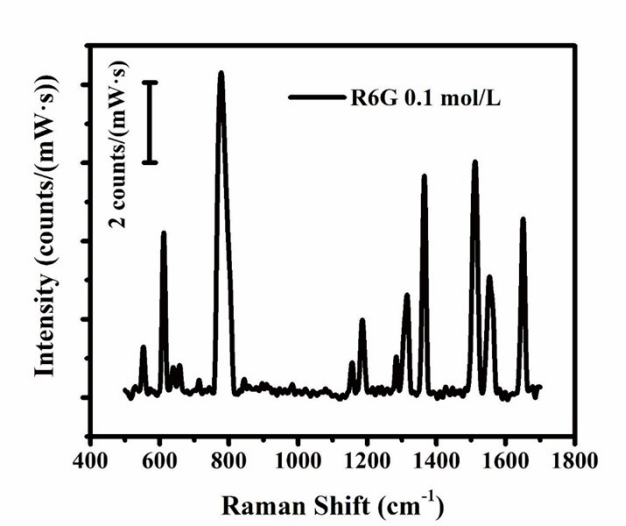

Fig. S8. The Raman spectrum of 0.1 mol/L R6G.

The EF was calculated by the widely used method[1-4], EF = (I_{SERS}/N_{SERS})/(I_{Raman}/N_{Raman}), where I_{SERS} and I_{Raman} are the normalized SERS intensity of AuNPs/R6G of 10^{-16} mol/L and Raman intensity of 0.1 mol/L R6G at 1360 cm^{-1}, and N_{SERS} and N_{Raman} are the molecules number of AuNPs/R6G of 10^{-16} mol/L and 0.1 mol/L R6G exposed to the laser focal area, respectively. The Raman spectrum of 0.1 mol/L R6G, as shown in Fig. S8, was obtained from a 2 μL droplet with the same measurement parameters except the exposure time (5s). The number of molecules exposed to the laser spot was calculated with the concentration multiplied by the ratio between the laser focal area (diameter of around 3 μm) and the individual sample area. The sample area is approximately 2×10^5 μm^2 of AuNPs/R6G under 5 cycles/s driving frequency and 12×10^5 μm^2 of R6G droplet for the static CR system, respectively, as shown in Fig. S5.

Section 2. COMSOL Model establishment for simulation

The model was established in a three-dimensional structure using COMSOL Multiphysics software. The gold nanospheres with diameter of 100 nm were

employed. The electric field distributions were calculated by Electromagnetic Waves (Frequency Domain) model with the following governing equations

$$\nabla \times \mu_r^{-1}(\nabla \times E) - k_0^2\left(\epsilon_r - \frac{j\sigma}{\omega\epsilon_0}\right)E = 0 \quad (1)$$

$$\nabla \times (\nabla \times E) - k_0^2\epsilon_r E = 0 \quad (2)$$

where ϵ_r is the relative permittivity, μ_r is the relative permeability, σ is the electrical conductivity, j is the current density and k_0 is the wave number. For convenient calculation, the periodic boundary conditions were set as continuity

$$E_{dst} = E_{src} \quad (3)$$

$$H_{dst} = H_{src} \quad (4)$$

where E and H are the electric field intensity and magnetic field intensity, respectively, the subscript '*dst*' and '*src*' refer to destination and source, respectively. In this model, all parameters were set approximately in accordance with the experimental conditions, with the excitation wavelength 633 nm, excitation power 4.25 mW and a typical electric mode field 1 V/m. To distinguish the SERS performance in CR and SCR system, a scattered distribution of monolayer consisted of 6 AuNPs (with the individual inter-gap of 50 nm, 100 nm and 325 nm, respectively) was employed as on the CR stain. In comparison, a uniform distribution of monolayer consisted of 10 AuNPs with the narrower inter-gap of 25 nm was also applied. The even distribution of 'hot-spots' can provide the reproducible and reliable Raman readouts. The narrower inter-gap also enables the stronger localized EMF for higher SERS property. To further evaluate the influence of AuNPs configuration in SCR system on the assembled 'hot-spots', the multilayer AuNPs (both double and triple layers based on the uniform monolayer) with inter-gap of 25 nm were employed. The highly condensed configuration of AuNPs not only improves the effective amounts of 'hot-spots', but also generates the stronger localized EMF, which

significantly contributes to the further enhancement of Raman signal compared with that on CR stain.

References

1. B. Ankudze, A. Philip and T. T. Pakkanen, *Anal. Chim. Acta*, 2019, **1049**, 179-187.
2. X. Liu, Y. Shao, Y. Tang and K. F. Yao, *Sci. Rep.*, 2014, **4**, 5835.
3. J. Ye, J. A. Hutchison, H. Uji-i, J. Hofkens, L. Lagae, G. Maes, G. Borghs and P. V. Dorpe, *Nanoscale*, 2012, **4**, 1606-1611.
4. G. Shi, M. Wang, Y. Zhu, L. Shen, Y. Wang, W. Ma, Y. Chen and R. Li, *Opt. Commun.*, 2018, **412**, 28-36.